International Journal of Signal Processing, Image Processing and Pattern Recognition
Vol.9, No.5 (2016), pp.399-416
http://dx.doi.org/10.14257/ijsip.2016.9.5.36

Super-Resolution Reconstruction based on Tukey Norm and Adaptive Bilateral Total Variation

Jie Shen[1, 2], Feng Xu[1], Mengxi Xu[3], Yun Yang[1], Ruili Wang[4] and Lili Zhang*[1]

1(College of Computer and Information Engineering, HoHai University, Nanjing, China)
2 (College of communication engineering, PLA University of Science and Technology, Nanjing, China)
3(School of Computer Engineering, Nanjing Institute of Technology, Nanjing , China)
4(School of Engineering and Advanced Technology, Massey University, Auckland, New Zealand)
** maple@hhu.edu.cn; jieshen_hhu@163.com*

Abstract

In Bilateral Total Variation (BTV) regularized super-resolution reconstruction (SRR), the fidelity item is only applicable to a specific noise model, and the fixed weight of BTV regularization term cannot adapt to the changes in an image. Thus, this paper proposes a SRR algorithm based on the Tukey fidelity term and adaptive BTV regularization term. The Tukey fidelity term has a more effective outliers suppression feature to deal with complex noises, and the weight of adaptive BTV regularization term can resize itself according to the changes of image textures, which can achieve the purposes of suppressing noises and preserving edges. Experimental results show that, compared with other algorithms, the proposed algorithm has better vision effects and higher Peak Signal-to-noise Ratio (PSNR) values.

Keywords*: Super-resolution; Image reconstruction; Tukey norm; BTV; Adaptive weight*

1. Introduction

Image super-resolution reconstruction (SRR) is a process that fuses low resolution (LR) images, combined with the certain priori, to reconstruct a high resolution (HR) image with more details [1-2]. Currently, SRR has been widely used in medicine, remote sensing, military surveillance, image compression and other imaging fields [3-6]. The concept of image SRR was firstly proposed by Tsai and Huang [7], then gradually developed [8]. Its early research focused on the frequency domain, but it is difficult to integrate into the image priors, so the current research mainly focuses on the spatial methods, which mainly include: non-uniform interpolation [9], the iterative back projection (IBP) [10], projection on convex sets (POCS) [11], the maximum a posteriori (MAP) method [12-13], the learning method [14], the regularization method [15-22], *etc.*

Image SRR is essentially a kind of inverse problem, which is often ill-posed. An effective way to solve the ill-posedness is regularization. He and Kondi [15] used L2 norm and Tickhonov regularization for SRR, which adopted an adaptive regularization parameter to adjust the weights of the LR frame in the reconstruction process; Ng *et al.* [16] proposed a SRR algorithm based on L2 norm and the Total variation (TV) regularization. Because the L2 fidelity term is especially sensitive to data which are not

*Corresponding Author

ISSN: 2005-4254 IJSIP

based on specific model, Farsiu and Robinson [17] proposed a SRR algorithm based on L1 norm and used the Bilateral Total Variation (BTV) operator as the regularization. To preserve the edge better, Li *et al.* [18] proposed a regularization method based on local adaptive BTV, and the experimental results verified the effectiveness of the improved algorithm; Yuan *et al.* [19] put forward a SRR algorithm based on the spatially weighted TV regularization. In order to improve the robustness of the algorithm, Patanavijit *et al.* [20] put forward a SRR algorithm based on Huber norm, and proposed the algorithm based on the Lorentzian norm in [21]. Pham *et al.* [22] proposed the algorithm based on gauss error norm which can more effectively suppress outliers. Patanavijit *et al.* [23] also combined the Tukey's Biweight norm and Tikhonov regularization to conduct image SRR, and the experimental results demonstrated the superiority of the proposed SRR to other SRR methods based on L1 and L2 norms.

Generally, fidelity terms in BTV regularized SRR algorithms are based on L1 or L2 norm for specific noise model, and are much sensitive to other model data. Besides, the fixed weight coefficient of BTV regularization cannot adapt to the changes of image details. In this paper, a SRR algorithm based on Tukey norm fidelity term and adaptive BTV regularization is proposed. Tukey norm fidelity term, which gives the outliers zero weight, is suitable for processing complex noise; while adaptive BTV regularization considers the gradient features of the input gray image based on BTV. By defining a quantity which is called Local Relative Gradient Difference (LRGD) we introduce the adaptive weight, which enhances the detail information in the reconstructed image. The algorithm can obtain better reconstruction results for different noise models, and can keep edges well.

2. Image Observation Model and Super-Resolution Reconstruction

Usually, p observed images can be obtained from the high-resolution image through the motion, blurring, downsampling, and noise-adding. The observation model [24] is expressed as:

$$Y_k = D_k H_k F_k X + E_k \qquad k = 1,2,..., p \tag{1}$$

Assuming p LR images known with size of $N_1 \times N_2$. They are arranged as vector Y_k with size of $N_1 N_2 \times 1$; X represents the original HR image with size of $L_1 N_1 \times L_2 N_2$. L_1 and L_2 are upsampling factors in row and column respectively. F_k and H_k represent the distortion matrix and blurring matrix (PSF) respectively with size of $L_1 N_1 L_2 N_2 \times L_1 N_1 L_2 N_2$; D_k is the downsampling matrix with size of $N_1 N_2 \times L_1 N_1 L_2 N_2$; E_k represents additive noise with size of $N_1 N_2 \times 1$.

According to imaging model proposed by Elad [25], when the imaging equipment and external conditions are fixed, the blurring matrix and the downsampling matrix are constant and used in p low-resolution images, that is $H_k = H$, $D_k = D$. Therefore, equation (1) can be written as:

$$Y_k = DHF_k X + E_k \qquad k = 1,2,..., p \tag{2}$$

According to the image observation model represented in equation (2), the task of SRR is to obtain the estimation of the original HR image by reconstructing the p observed LR images, which is typically an inverse problem. The cost equation based on the MAP framework is as follows:

$$J(X) = \sum_{k=1}^{p} \left\| DHF_k X - Y_k \right\|_l^l \tag{3}$$

Then, the problem that SRR needs to solve is to minimize the cost equation above with respect to X . The corresponding expression is as follows:

$$X = \arg\min_{X} J(X) \tag{4}$$

3. Tukey Norm

To make the cost function convex, generally the value range of l is limited to $1 \le l \le 2$. Also, to simplify the calculation, $l = 1$ or $l = 2$, namely, L1 norm or L2 norm is adopted. L2 norm is the optimal estimation corresponding to Gaussian noise, which is extremely sensitive to abnormal values caused by the outliers. When there are other kinds of noises, the effect of reconstruction is poor. Meanwhile it can cause over-smoothing to images. L1 norm is the maximum likelihood estimation for the Laplace noise model[17]. Compared with L2 norm, L1 norm can effectively remove the influence of outliers. But when the noise satisfies the Gaussian distribution, the result deviates greatly. L1 norm can preserve the image details, but in a flat area it can cause contour effect, which leads to the distortion on the image. Apparently, the L1 norm and L2 norm both have some limitations.

In 1996, Black [26] proposed the M-estimation to restore image for the first time. M-estimation is a commonly used method in the field of statistics, which is an extension of the classical maximum likelihood (ML) estimation. It has the advantages of low complexity and good robustness, therefore, it has been widely used in image processing. In the cost function, the M-estimation norm can guarantee the image details, while effectively suppress outliers. In M-estimation the common used norms are Huber norm, Lorentzian norm, Tukey norm, *etc.*

SRR based on norm estimation can be formulated as a more general form:

$$X = \arg\min_{X} \sum_{k=1}^{P} \rho(DHF_k X - Y_k) \tag{5}$$

Where $\rho(\bullet)$ represents the consistency between observation and real data, namely it takes a certain method to measure the distance between the two quantities. To minimize $\sum_{k=1}^{P} \rho(DHF_k X - Y_k)$, $\rho(\bullet)$ we selected should be able to minimize the effect of $(DHF_k X - Y_k)$ on the measurement, namely a small weight should be given when $(DHF_k X - Y_k)$ is large to some extent. Changes in weights can be seen from the influence function $\psi(\bullet)$ which is obtained from derivation calculus to norm $\rho(\bullet)$. The formulas of the functions $\rho(\bullet)$ and their influence functions $\psi(\bullet)$ are expressed in Table 1, where σ is called the scale factor.

And the corresponding graphs of the influence functions are shown in Figure 1.

Whether the influence function of the norm is continuously bounded can determine robustness of the estimation method. If the influence function is continuously bounded, outliers won't result in noticeable deviation in estimation results. As can be seen, the influence function of L2 norm is unbounded, which is different from M-estimation. When the residual continuously increases, the value of L2 norm influence function is of linear growth, resulting in serious deviation.

Table 1. Formulas of the Norms and Their Influence Functions

Function types	$\rho(x)$	$\psi(x)=\rho(x)$
L2	$x^2/2$	x
L1	$\lvert x\rvert$	$sign(x)$
Huber $\begin{cases}\lvert x\rvert\le\sigma\\ \lvert x\rvert>\sigma\end{cases}$	$\begin{cases} x^2/2 \\ \sigma\lvert x\rvert-\sigma^2/2\end{cases}$	$\begin{cases} x \\ \sigma\, sign(x)\end{cases}$
Lorentzian	$\frac{\sigma^2}{2}\log[1+(x/\sigma)^2]$	$\frac{x}{1+(x/\sigma)^2}$
Tukey $\begin{cases}\lvert x\rvert\le\sigma\\ \lvert x\rvert>\sigma\end{cases}$	$\begin{cases}\frac{\sigma^2}{6}\left\{1-\left[1-(x/\sigma)^2\right]^3\right\} \\ \sigma^2/6\end{cases}$	$\begin{cases} x\left[1-(x/\sigma)^2\right]^2 \\ 0\end{cases}$

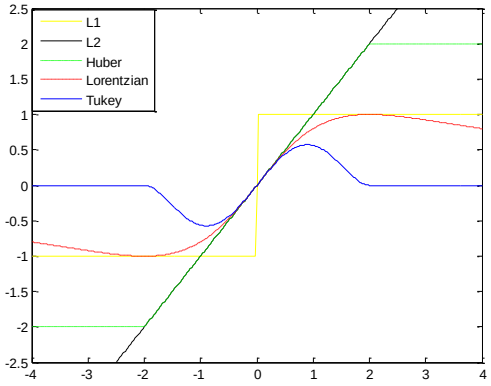

Figure 1. The Influence Functions of Norms

According to the bounded influence function, M-estimation can be divided into 3 categories [27]:

1) M-estimation method with the monotonic influence function: when the residual is greater than the threshold, influence function is constant, that is, uniform weighted values are distributed to the observation. L1 and Huber estimation belong to this type of M-estimation method.

2) M-estimation method with soft fall back influence function: when residual tends to infinity, influence function is close to 0. Lorentzian estimation belongs to this kind of M-estimation method.

3) M-estimation method with hard fall back influence function: when residual is greater than the threshold, influence function is rapidly weakened to 0. Tukey estimation is one of them.

Along with the increase of the residuals, the values of influence function in the second and the third types of estimation methods decrease. Then the outliers' influence on the estimation also gradually decrease, thus, the M-estimation with fall back influence function has better robust performance. Tukey norm has hard fall back influence function which will rapidly approach to 0 when the residual is greater than the threshold, that is, zero weight is given to the outlier. Thus Tukey norm can suppress the outliers better. Therefore, this paper introduces the Tukey norm in M-estimation that has a better robust performance to replace the commonly used L1 and L2 norms.

In M-estimation, the scale factor σ is the threshold value that is able to distinguish between outliers and model data. Namely, when the absolute value of the residual $|x|$ of the observation data is greater than σ, the observation data is identified as an outlier. When $|x|$ is less than σ, Tukey norm is approximately equivalent to the L2 norm, which can smooth the image. Contrarily, when $|x|$ is greater than σ, namely, the outlier appears, the value of the influence function approach to 0 rapidly, which means zero weight is given to the outlier. That is, outliers can be strongly suppressed. Thus it can more effectively improve the robustness of the algorithm by introducing Tukey norm into the data fidelity term.

The selection of σ has a great influence on the effect of the algorithm. There are a variety of criteria for judgment of outliers, such as Pauta criterion, Chauvenet criterion, Grubbs criterion, *etc.* The Median Absolute Deviation (MAD) method proposed in [28] is used to select the value of σ in this paper, which is simple in calculation and easy to be understood. Comparison of the relative performance of the selection methods of σ will be validated in the experimental section. The formula is:

$$\sigma_{\varepsilon} = 1.4826MAD(\nabla I) = 1.4826median\{|\nabla I - median(\nabla I)|\} \tag{6}$$

Where ∇I represents the set of observation data.

4. SRR Algorithm Based on BTV Regularization

Considering the existence of all kinds of noises, as the blurring matrix is a highly ill-posed sparse matrix [29], the SRR is typically an ill-posed inverse problem. That is, the solution of the equation cannot meet the three conditions: the existence, the uniqueness and the stability. In 1977, Tikhonov proposed the regularization method to solve the ill-posed problem [30]. By introducing regularization term into the cost equation, solution space can be restrained, the influence of noise can be minimized, and solution of the inverse problem can be stabilized, which makes the problem a well-posed one with a unique solution. Regularization term is generally composed of image prior information such as image gray scale information and edge information, which is usually in the form of penalty function in the cost function. The cost equation with regularization term is as follows:

$$J(X) = \sum_{k=1}^{p} \rho(DHF_k X - Y_k) + \lambda\gamma(X) \tag{7}$$

Where the first term is called the fidelity term, which reflects the fitting degree between the observation data and the original data. The second term is the regularization item, which represents the constraints to regularity of the solution such as smoothness. λ is the regularization parameter, which is used to adjust the relative influence of the two terms above on the reconstruction image. If λ is too large, the high frequency information will decrease greatly, which will make the image details missing and the reconstruction image too smooth. If λ is too small, the fidelity of the image is too high, which cannot restrain noise and eliminate the ill-posedness well.

The design of the regularization term directly affects the reconstruction effect. At present, the commonly used regularization terms are Tikhonov regularization, the Total Variation (TV) regularization, and Bilateral Total Variation (BTV) regularization. BTV has the constraints to spatial relationships as well as gray relationships between image pixels, thus BTV regularization can suppress noise while better maintain image edge features.

BTV regularization can be expressed as follows[17]:

$$\gamma_{BTV}(X) = \sum_{l=-p}^{p} \sum_{m=0}^{p} \alpha^{|m|+|l|} \left\| X - S_x^l S_y^m X \right\|_1 \tag{8}$$

where, S_x^l and S_y^m respectively represent matrix operators in the horizontal direction translating l pixels and in the vertical direction translating m pixels; $\left\| X - S_x^l S_y^m X \right\|_1$ represents the difference of X in different scales; α is the weight coefficient, and $0 < \alpha < 1$.

5. SRR Algorithms based on Tukey Norm Fidelity Term and Adaptive BTV Regularization

The size of the weight coefficient α for BTV regularization has an important influence on keeping the image local details. On the one hand, smaller α can sharpen image edge well, but can bring a lot of noise to the image; on the other hand, larger α can effectively suppress the influence of noise, but will cause the image edge blur. Therefore, how to select the appropriate α is very important. The adaptive weight $\alpha(i, j)$ is introduced in this paper, namely each pixel has a different weight. Weights are selected according to the local gray features of different pixel points. The smaller value is selected for the area with rich details; the larger value is selected for the area with flat grey values.

In this paper, we use $z(i, j)$ defined in (11) to quantitatively represent the flatness of the area, and we define it as Local Relative Gradient Difference (LRGD). We use the way of local window to calculate the value. The size of the selected local window is $M = (2P+1)(2Q+1)$, in this paper we set $P = Q = 2$.

$$z(i, j) = \frac{1}{M} \sum_{s=i-P}^{i+P} \sum_{t=j-Q}^{j+Q} \left| X(s,t) - \bar{x}(i, j) \right| \tag{9}$$

$$\bar{x}(i, j) = \frac{1}{M} \sum_{s=i-P}^{i+P} \sum_{t=j-Q}^{j+Q} X(s,t) \tag{10}$$

Where $\bar{x}(i, j)$ represents the local gray average, and $z(i, j)$ represents the LRGD value of the HR image in the area of (i, j). However, in many cases, the original HR image has not been given, so $z(i, j)$ in formula (11) cannot be calculated, thus limiting the application of this method. In this case, the initial HR image X_0 obtained by the spline interpolation can be taken to replace the original HR image. Large $z(i, j)$ indicates that there is large difference within pixels, which means smaller α is needed to sharpen the edge; and vice versa. So we can see that weight $\alpha(i, j)$ has negative relation with $z(i, j)$. $\alpha(i, j)$ is taken as following:

$$\alpha(i, j) = \frac{1}{1 + z(i, j)} \tag{11}$$

It is easily seen that $\alpha(i, j)$ meets the condition $0 \le \alpha \le 1$.

It is assumed $A = diag\left(\alpha_1^{|m|+|l|}, \alpha_2^{|m|+|l|}, ..., \alpha_{L_1 N_1 \times L_2 N_2}^{|m|+|l|}\right)$, which is called adaptive weight matrix. BTV regularization with the introduction of adaptive weight matrix is as follows:

$$\gamma_{SBTV}(X) = \sum_{l=-p}^{p}\sum_{m=0}^{p}\left\|A\left(X - S_x^l S_y^m X\right)\right\|_1 \tag{12}$$

Then, the cost function of SRR algorithm based on the Tukey norm fidelity term and adaptive BTV regularization is expressed as:

$$J(X) = \sum_{k=1}^{p}\rho_{Tukey}\left(DHF_k X - Y_k\right) + \lambda\sum_{l=-p}^{p}\sum_{m=0}^{p}\left\|A\left(X - S_x^l S_y^m X\right)\right\|_1 \tag{13}$$

The steepest descent method is used to minimize the cost equation. After derivation calculus to $J(X)$, we can get:

$$\nabla_X J(X) = \sum_{k=1}^{p} F_k^T H^T D^T \bullet \psi_{Tukey}\left(DHF_k X - Y_k\right) + \lambda\sum_{l=-p}^{p}\sum_{m=0}^{p}\left(I - S_x^{-l} S_y^{-m}\right) Asign\left(X - S_x^l S_y^m X\right) \tag{14}$$

Then the successive iteration is conducted, and the final iteration formula is:

$$X_{n+1} = X_n - \beta\left\{\begin{array}{l}\sum_{k=1}^{p} F_k^T H^T D^T \bullet \psi_{Tukey}\left(DHF_k X_n - Y_k\right) \\ +\lambda\sum_{l=-p}^{p}\sum_{m=0}^{p}\left(I - S_x^{-l} S_y^{-m}\right) Asign\left(X_n - S_x^l S_y^m X_n\right)\end{array}\right\} \tag{15}$$

Where β is the iteration step. In order to accelerate the convergence of the algorithm, larger β is generally selected at the beginning of the iteration, then the value is gradually reduced to improve the precision of the algorithm.

In conclusion, the basic steps of the SRR algorithm proposed are as follows:

1) The low-resolution images after image registration are projected to the grid of high resolution image, then the spline interpolation is implemented to obtain the initial high-resolution image X_0 and the number of iterations is initialized as $n = 0$;

2) The gradient $\nabla_X J(X_n)$ of the cost function $J(X)$ in the nth iteration is solved;

3) The current high resolution image is iteratively updated, $X_{n+1} = X_n - \beta\nabla_X J(X_n)$;

4) The terminating condition is determined:

If $\frac{\left\|X_{n+1} - X_n\right\|_2^2}{\left\|X_n\right\|_2^2} \leqslant \eta$, the iteration is terminated and X_{n+1} is obtained as the final HR image; Otherwise, set $n = n+1$, and skip to step 2) to continue with iteration. η is the preset threshold.

6. Experimental Results and Analysis

Mean Square Error(MSE), Signal-to-noise Ratio(SNR) and Peak signal-to-noise Ratio(PSNR) are the most commonly used evaluation criteria of image and video quality. In this paper, PSNR is used to quantitatively estimate the quality of image reconstruction, which has simple algorithm and clear physical meaning. And the terminating condition is set: $\frac{\left\|X_{n+1} - X_n\right\|_2^2}{\left\|X_n\right\|_2^2} \leqslant 10^{-4}$.

Firstly, In order to verify the impact of the scale factor σ on the algorithm performance and the relative superiority of the MAD method, we conduct a set of simple experiment.

256× 256 Camera image is chosen, first we use the symmetric Gaussian lowpass filter of size 5× 5 with standard deviation 1 to blur the original image, then shift it in the horizontal and vertical direction ranging from 1 to 2 pixels which are randomly obtained, next we downsample the image with the sampling factor of 2 to get 4 LR images with the size of 128× 128. To compare the ability of the algorithm to suppress outliers more intuitively, we add salt and pepper noise whose density is 0.01 to the LR images. And we guarantee that other parameters are set consistent in the experiment: $\lambda = 0.1, \alpha = 0.7, \beta = 1, p = 2$. Figure 2 shows the experimental results of the Tukey algorithm with different selection methods of σ : (a) represents the LR image, (b) represents the result of spline interpolation amplification, Figure (c) represents the result of Tukey algorithm with Median method, which means the median of the pixel values of the HR image x_n obtained from each iteration is assigned to σ to conduct the next iteration, (d) represents the result with Mean method, which uses the mean of the pixel values of the HR image x_n obtained from each iteration to substitute σ , (e) shows the result of Tukey algorithm with the fixed constant σ , where we use the mean of the result of the spline interpolation x_0 to assign σ , and (f) represents the result of Tukey algorithm with the MAD method we mentioned above. And Table 2 lists the corresponding PSNR values.


(a) LR image


(b) Spline interpolation


(c) Median method


(d) Mean method


(e) Fixed constant method

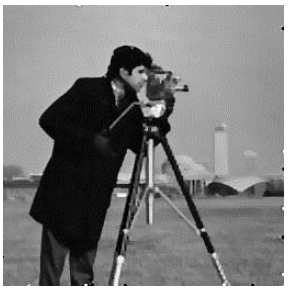
(f) MAD method

Figure 2. SRR Results with Different Selection Methods of σ

Table 2. PSNR Values for Reconstruction Results (Unit: dB)

	Spline interpolation	MAD method	Median method	Mean method	Fixed constant method
PSNR	19.7351	22.0726	21.2276	21.3479	21.3571

Of course, it can be seen from Figure 2, compared with the spline interpolation the reconstruction effects of Tukey algorithms with different methods of choosing σ have improved to some extent. Figure (c) has more faint spots compared with (d) , (e) and (f), which affects the image quality. That is, from visual effects the result of Tukey algorithm with Median method is worse than those of Tukey algorithms

with Mean method, Fixed constant method, and MAD method. Although it looks that the effect of (e) is better than that of (d), σ in Figure (e) is a constant obtained by x_0, which cannot adjust itself with the iteration. Thus the effect of the Fixed constant method cannot be determined. By comparison, we can see that Figure (f) is clearest and has more significant details. Particularly in the face of the man, Figures (c), (d) and (e) are relatively vague, let alone the edges of the man and the tripod of the camera. The values in Table 2 are consistent with the visual effects. PSNR value of the Tukey algorithm with MAD method is relatively higher than those of the other methods. So the effect of MAD method is better compared with the other methods, which can better suppress outliers and maintain image edges and details. Thus, we use the MAD method to choose σ in the following experiments.

Then with the above experimental data we verify the effect of different selection of regulation parameter $\lambda \frac{n!}{r!(n-r)!}$ on the reconstruction of the Tukey algorithm. The corresponding results are shown below, which are PSNR values of reconstruction images obtained by different λ.

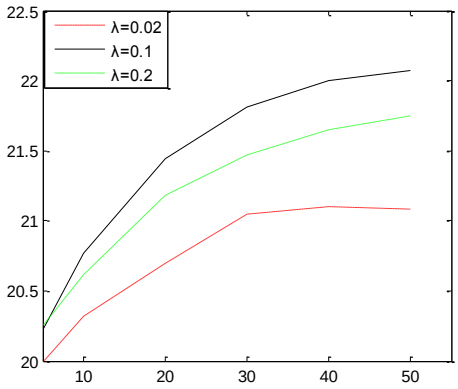

Figure 3. PSNR Values for Reconstruction Results of Different λ

As can be seen from the figure, the appropriate selection of λ can effectively improve the quality of image reconstruction. In this experiment, PSNR values are largest when $\lambda = 0.1$, too small λ cannot restrain noise and eliminate the ill-posedness well, too large λ results in the loss of image details. Both cases degrade the quality of the reconstructed image.

In order to verify the validity of the proposed algorithm in this paper, the image spline interpolation amplification, BTV algorithm based on L2 norm (L2 + BTV), BTV algorithm based on L1 norm (L1 + BTV), BTV algorithm based on Tukey norm (Tukey + BTV) and the algorithm proposed in this paper (Tukey + SBTV) are respectively implemented. Basic comparison is with the spline interpolation amplification, and the selection of BTV algorithm based on L2 norm and L1 norm is to verify the effectiveness of the introduction of the Tukey norm fidelity term. The comparison between the proposed algorithm and Tukey-based BTV algorithm illustrates the effectiveness of the adaptive BTV. In the experiment, the iterative step β we selected declines from 1.0 to 0.1 gradually.

Lena image is selected, the size of which is 256×256. According to the observation model, the image is respectively blurred, translated, downsampled, and degraded by noise to generate 4 LR images with the size of 128×128, where the averaging blur operator is 3×3, translation ranges from 1 to 2 pixels, and the coefficient of downsampling is 2.

To compare the robustness of different algorithms, we apply 5 kinds of reconstruction algorithms respectively to the gaussian noise model, salt and pepper noise model and hybrid noise model containing two kinds of noises to conduct the contrast experiments. In Figure 4 we add Gaussian white noise of mean 0 and variance 40 to the images. Salt and pepper noise whose density is 0.01 is added to the LR images in Figure 5. In Figure 6, the two kinds of noises are included. Figures 4, 5, and 6 are respectively LR images with different noises and the reconstruction results of 5 kinds of algorithms, and Table 3 shows the PSNR values obtained by different reconstruction algorithms. In the experiment we set: $\lambda = 0.1, p = 2$, and for all the other BTV algorithms α is 0.7 except the proposed algorithm, which is adaptive.

From visual effects, Figures (b) in the above three groups of images, which are the results of the spline interpolation, have the worst effects for no priori introduced. They are used as the initial HR images X_0 of BTV algorithms in this paper, which have odd anomalies along the edges. Thus, BTV algorithms can be compared on the unified basis of X_0, and the edges of some of the results of the algorithms also appeared outliers, by which can better reflect the capacity of outliers suppression of different algorithms. Figures (e) have better effects than those of Figures (c) and (d) in each set of images, which show clearer images, more obvious outlines and less outliers along the edges. Thus the algorithm based on Tukey norm has better visual effects than those of algorithms based on L2 norm and L1 norm, which means the algorithm can effectively suppress the noises, and maintain image edges to a certain extent. The algorithm based on Tukey norm has better reconstruction results for LR images with different noises, especially in Figure 5, LR images with salt and pepper noise, image restoration effect is more obvious. It demonstrates the superiority of Tukey-based method for suppressing outliers, and the algorithm can be applied to different noise models.

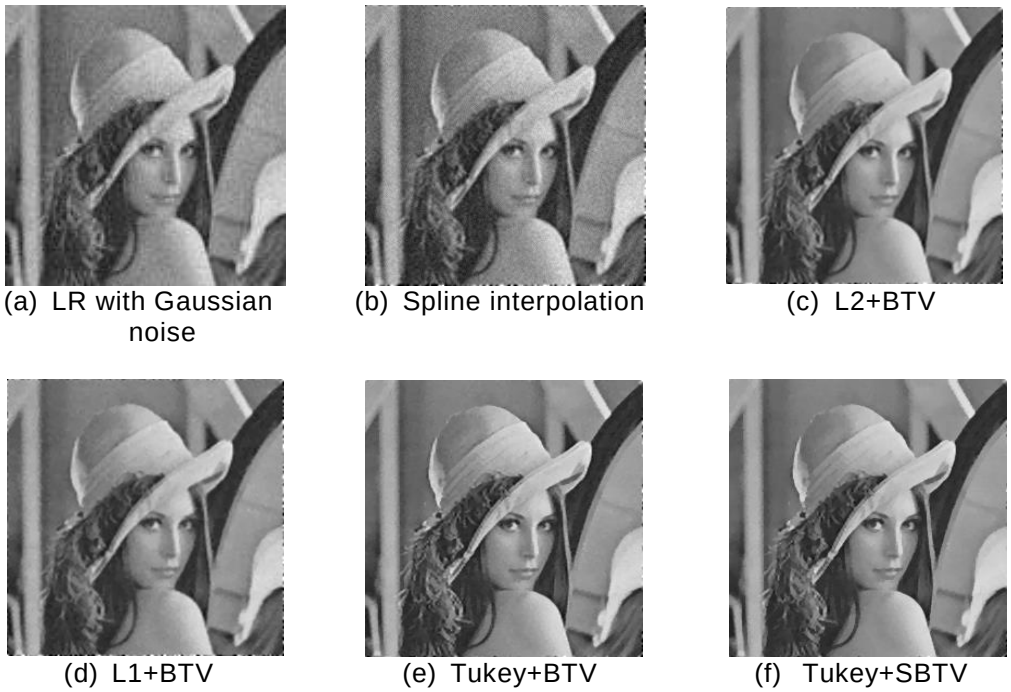

(a) LR with Gaussian noise (b) Spline interpolation (c) L2+BTV

(d) L1+BTV (e) Tukey+BTV (f) Tukey+SBTV

Figure 4. SRR Results for Gaussian Noise

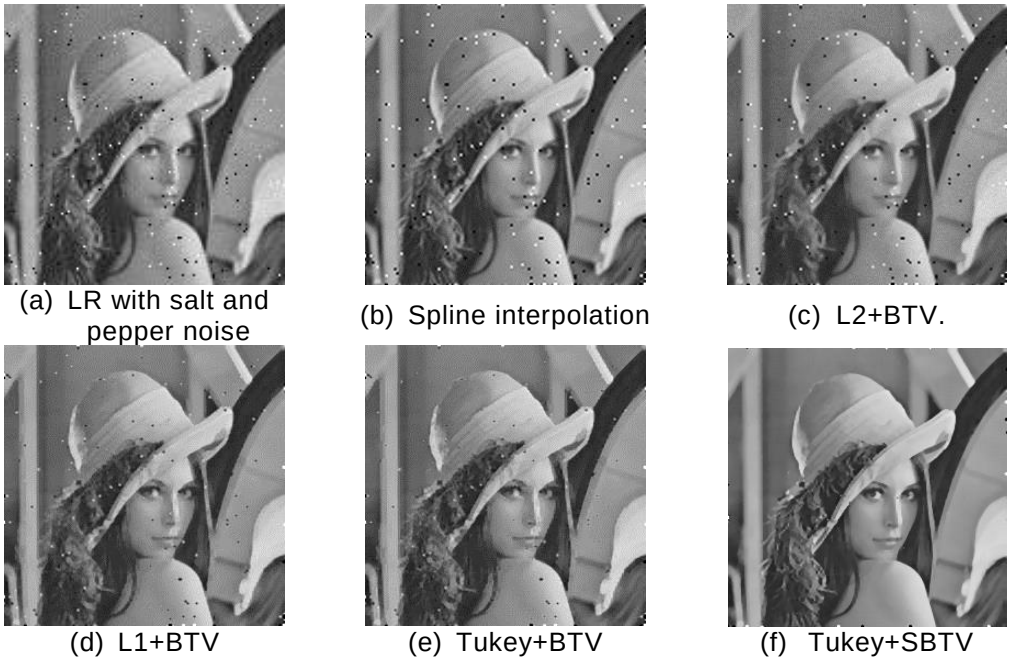

(a) LR with salt and pepper noise (b) Spline interpolation (c) L2+BTV.

(d) L1+BTV (e) Tukey+BTV (f) Tukey+SBTV

Figure 5. SRR Results for Salt and Pepper Noise

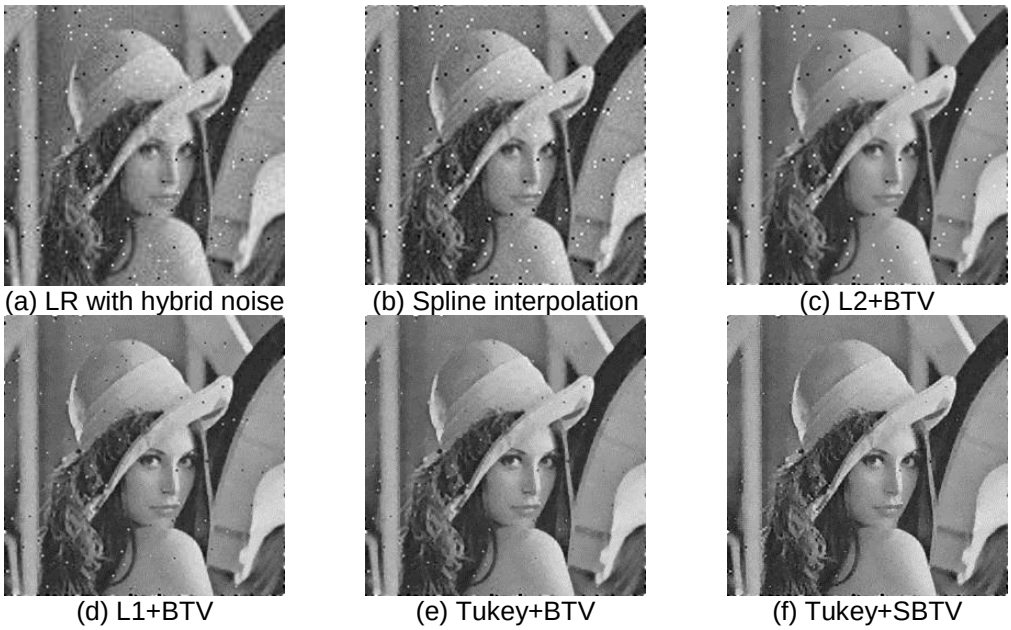

(a) LR with hybrid noise (b) Spline interpolation (c) L2+BTV

(d) L1+BTV (e) Tukey+BTV (f) Tukey+SBTV

Figure 6. SRR Results for Gaussian Noise Plus Salt and Pepper Noise

Figures (e) and (f) in the three groups of images are both based on the Tukey norm. From the comparison, it can be seen that Figures (f) have more clear details and better noise suppression effect than Figures (e), which shows the abilities of adaptive BTV regularization to keep local details and to suppress noises. And there are almost no odd anomalies along the edges in Figures (f), which fully demonstrates the ability of the proposed algorithm to remove outliers.

Table 3 lists the PSNR values of the reconstruction results in different algorithms, which are in keeping with visual effects. The PSNR values of spline

interpolation are the smallest. The PSNR values of BTV algorithm based on Tukey norm are improved comparing with those of the original BTV algorithms based on L2 norm and L1 norm, and the PSNR values of adaptive BTV algorithm based on Tukey norm is improved comparing with the BTV algorithm based on Tukey norm.

Table 3. PSNR Values for Reconstruction Results of Different Algorithms (Unit: dB)

	Gaussian noise (var=40)	Salt and pepper noise (D=0.01)	Hybrid noise (var=40,D=0.01)
Spline interpolation	23.4183	19.6537	20.5993
L2+BTV	24.1061	20.2832	20.9284
L1+BTV	23.9628	21.0415	21.5511
Tukey+BTV	24.5394	22.1743	22.6745
Tukey+SBTV	24.7803	22.7940	23.1749

In order to verify the applicability and effectiveness for the reconstruction of different images by the algorithm proposed, the remote sensing image of 256×256 is set to conduct the experiment above. We obtain 4 LR images of size 128×128 with the same operation as the previous experiment, where 3×3 Gaussian blur kernel is selected to degrade the image, translation ranges from 1 to 2 pixels, and the downsampling factor is 2. Gaussian white noise we added is of mean 0 and variance 40, and Salt and pepper noise we adopted is of density 0.01. The reconstruction results of LR images with different noises by different algorithms respectively are shown in the following three groups of images. The corresponding PSNR values of different reconstruction algorithms are listed in Table 4. In the experiment we set: $\lambda = 0.08, p = 2$, and α is set to 0.7 except the proposed algorithm, which is adaptive.

Apparently, as shown in Table 4, the experimental data results are consistent with the visual effects. Compared with other algorithms, the proposed algorithm has better reconstruction effects for LR images with different noises. Similarly, since the BTV algorithms are all based on the results of spline interpolation, odd anomalies along the edges still remain in the reconstruction results of some algorithms. As is shown, the outliers along the edges of the results of Tukey-based algorithm have been greatly reduced, let alone the proposed algorithm. The reconstruction results by algorithm based on Tukey norm are better than those by algorithms based on L2 norm and L1 norm. The proposed algorithm can effectively suppress the noise, make image clearer and obtain higher PSNR values. By the adaptive BTV algorithm based on Tukey norm, to which the adaptive weight coefficient is introduced, more image details are recovered and better edge-preserving is verified from visual effects, and the corresponding PSNR values have improved.

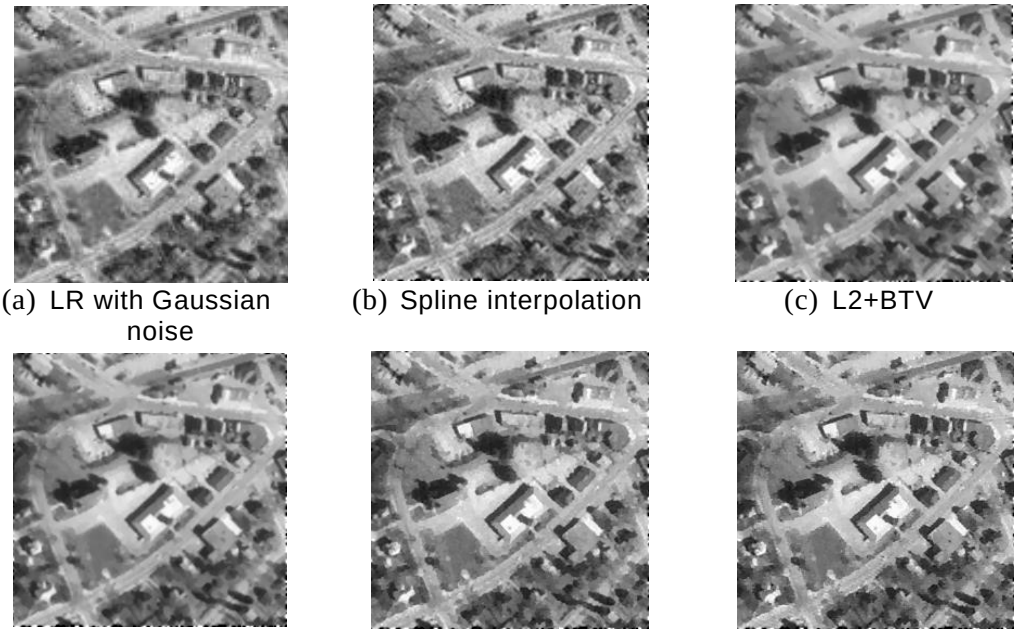

(a) LR with Gaussian noise (b) Spline interpolation (c) L2+BTV

(d) L1+BTV (e) Tukey+BTV (f) Tukey+SBTV

Figure 7. SRR Results for Gaussian Noise

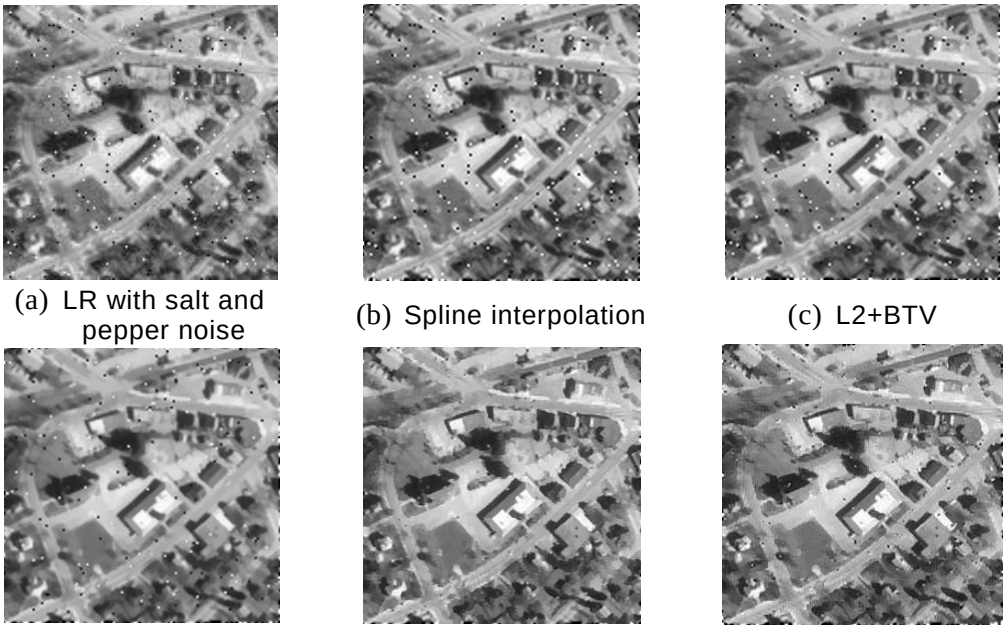

(a) LR with salt and pepper noise (b) Spline interpolation (c) L2+BTV

(d) L1+BTV (e) Tukey+BTV (f) Tukey+SBTV

Figure 8. SRR Results for Salt and Pepper Noise

(a) LR with hybrid noise (b) Spline interpolation (c) L2+BTV

(d) L1+BTV (e) Tukey+BTV (f) Tukey+SBTV

Figure 9. SRR Results for Gaussian Noise Plus Salt and Pepper Noise

Table 4. PSNR Values for Reconstruction Results of different Algorithms (Unit: dB)

	Gaussian noise (var=40)	Salt and pepper noise (D=0.01)	Hybrid noise (var=40,D=0.01)
Spline interpolation	22.1908	20.0866	19.4423
L2+BTV	22.8819	20.7650	19.8224
L1+BTV	22.5271	21.5053	20.3043
Tukey+BTV	23.5826	22.5692	21.3431
Tukey+SBTV	23.7860	23.0507	22.7127

The SRR by the image containing texts is used to verify the improvement of the reconstruction effects of the proposed algorithm below. Similarly, a series of degradation operation are implemented to produce 4 LR images of size 128×128, where 5×5 Gaussian blur operator is adopted, translation also ranges from 1 to 2 pixels, and the downsampling factor is 2. In the experiment Gaussian white noise we added is of mean 0 and variance 80, and Salt and pepper noise is of density 0.02. Image reconstruction results of different algorithms with different noises are shown in the figures below, Table 5 lists the corresponding PSNR values. Experimental parameters are set below: $\lambda = 0.06, p = 2$, and α is 0.7 except the adaptive algorithm we proposed.

From visual effects, the reconstruction effect of the image with salt and pepper noise by the algorithm based on L1 norm is better than that of the algorithm based on L2 norm. But to the images with other noises, the reconstruction effects by the algorithms based on L1 norm and L2 norm are similar. With different noises, the effects of the SRR based on Tukey norm are significantly better than those of algorithms based on L1 and L2 norm, which means the images are clearer and noises are suppressed more obviously. The results of the adaptive reconstruction algorithm introduced are the best. Compared with the algorithm based on Tukey norm, the texts are clearer and the noise suppression is better, which means the abilities of denoising and detail-preserving have been improved. Meanwhile, the odd anomalies along the edges are almost eliminated, which verifies the capacity of the proposed algorithm to suppress outliers. The PSNR values of the results listed in Table 5 are consistent with the visual effects. The PSNR values of algorithm based on Tukey norm are higher than those of algorithms based on L1 and L2 norm, while the PSNR values of the proposed algorithm are improved compared with algorithm based on Tukey norm.

In conclusion, compared with other four kinds of reconstruction algorithms, the proposed algorithm can obtain better visual effects and higher PSNR values, and can be well adapted to SRR with different noise models, which verifies the effectiveness of the algorithm proposed in this paper.

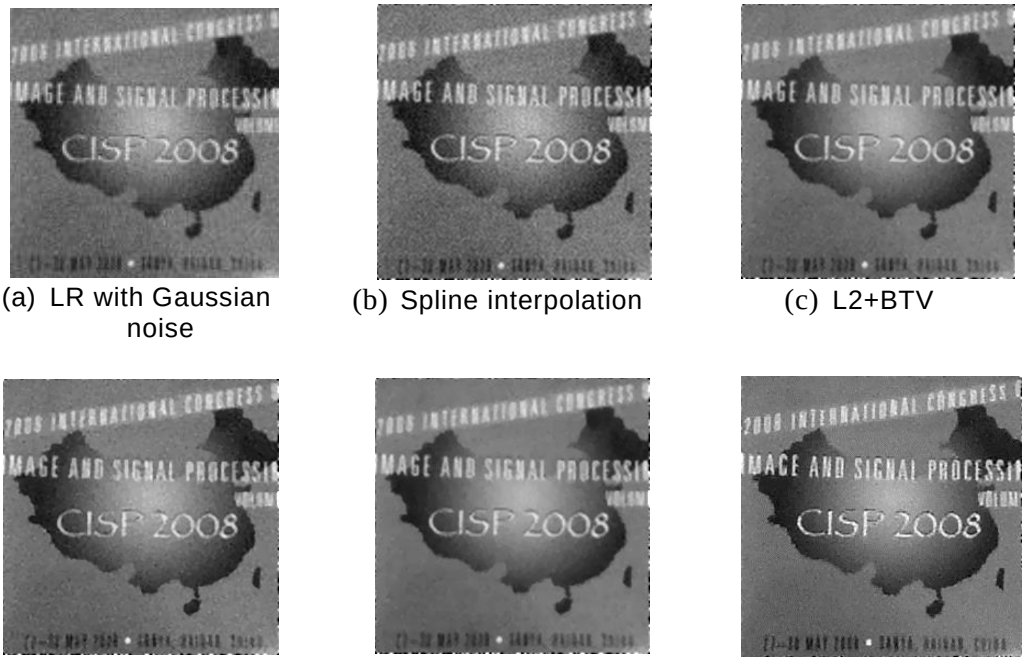

(a) LR with Gaussian noise (b) Spline interpolation (c) L2+BTV

(d) L1+BTV (e) Tukey+BTV (f) Tukey+SBTV

Figure 10. SRR Results for Gaussian Noise

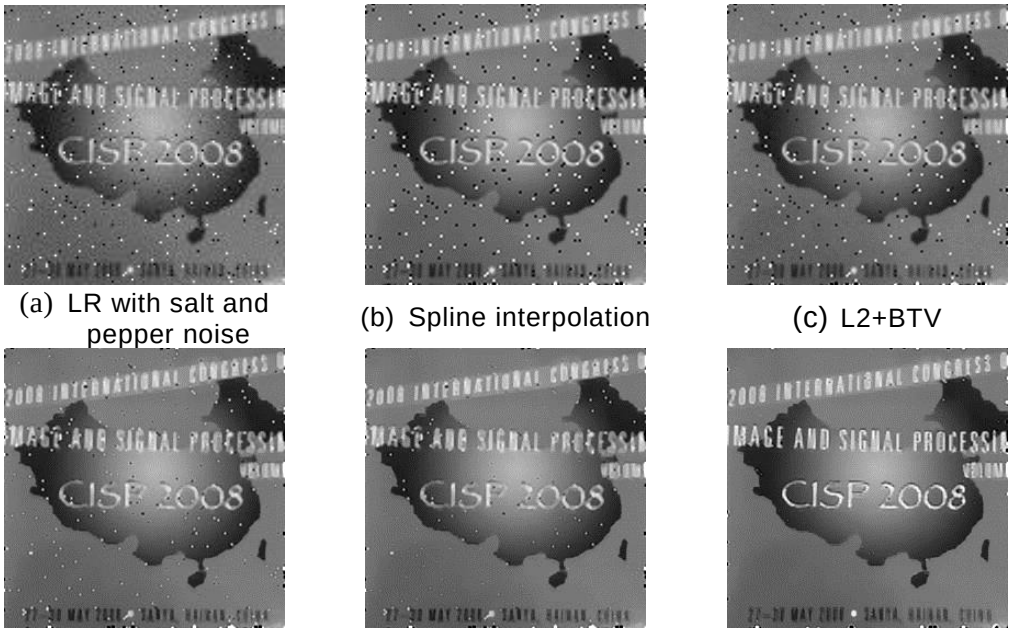

(a) LR with salt and pepper noise (b) Spline interpolation (c) L2+BTV

(d) L1+BTV (e) Tukey+BTV (f) Tukey+SBTV

Figure 11. SRR Results for Salt and Pepper Noise

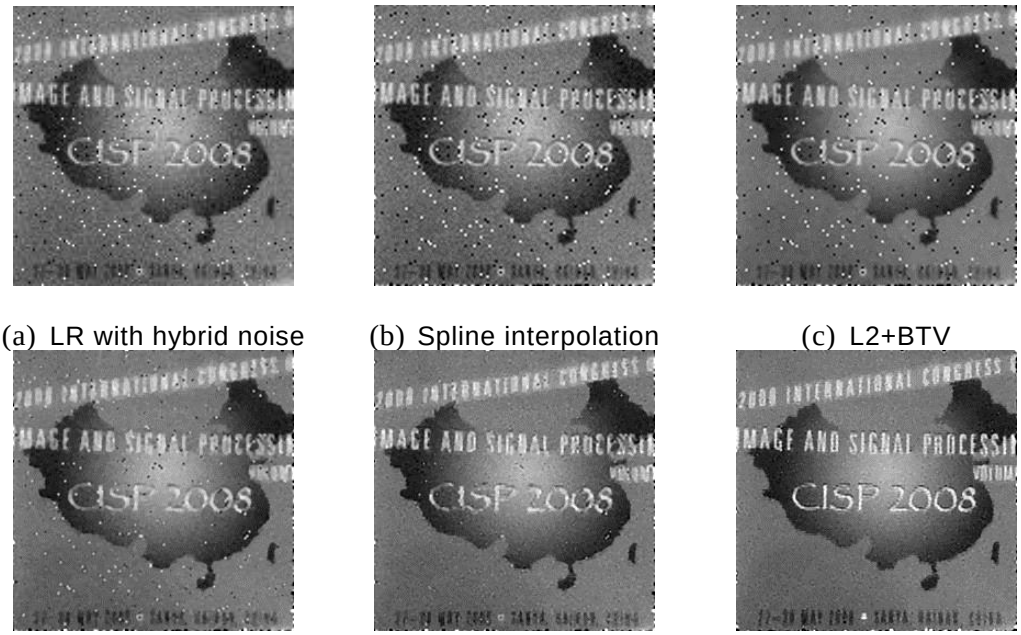

(a) LR with hybrid noise (b) Spline interpolation (c) L2+BTV

(d) L1+BTV (e) Tukey+BTV (f) Tukey+SBTV

Figure 12. SRR Results for Gaussian Noise Plus Salt and Pepper Noise

Table 5. PSNR Values for Reconstruction Results of Different Algorithms (Unit: dB)

	Gaussian noise (var=80)	Salt and pepper noise (D=0.02)	Hybrid noise (var=80,D=0.02)
Spline interpolation	21.6826	18.5408	18.8151
L2+BTV	22.2150	18.8375	19.0922
L1+BTV	22.0319	19.3986	19.8612
Tukey+BTV	22.8747	20.9389	20.5337
Tukey+SBTV	22.9801	21.3370	20.8807

7. Conclusion

In this paper, the SRR algorithm based on the Tukey fidelity term and adaptive BTV regularization is proposed. In the algorithm, the fidelity term is based on Tukey norm with better robustness feature which is suitable for suppressing complex noises. The adaptive BTV regularization considers the gradient features of the input gray image. By the adaptive weight coefficients, the details of the reconstruction image are further enhanced, which can make the reconstruction better. The proposed algorithm, which can be applied to different noise models, has higher PSNR values and better visual effects compared with other algorithms. The robustness and the edge-preserving properties of the algorithm are improved. However, the algorithm also exists the shortcomings of high computational complexity and slow convergence speed. How to eliminate these shortcomings still needs further study.

Acknowlegdements

This work is supported by the National Natural Science Foundation of China (No.61401195, No. 61374019), the Natural Science Foundation of Jiangsu Province (No.BK20130851), and the Natural Science Foundation of Jiangsu Higher Education Institutions (No. 13KJB520009).

References

[1] P. Milanfar, " Super-resolution imaging", CRC Press, New York, **(2010)**.
[2] Z. Xiong, X. Sun and F. Wu, "Robust web image/video super-resolution", IEEE Trans. Image Processing, vol. 19, no. 8, **(2010)**, pp. 2017-2028.
[3] M. X. Xu and C. G. Wei, "Remotely sensed image classification by complex network eigenvalue and connected degree", Computational and mathematical methods in medicine, id: 632703, **(2012)**.
[4] H. B. Wang, S. N. Zheng and X. Wang, "An approach for target detection and extraction based on biological vision", Intelligent Automation & Soft Computing, vol. 17, no. 7, **(2011)**, pp. 909-921.
[5] C. Wang, M. X. Xu, X. Wang, S. N. Zheng and Z. L. Ma, "Object-oriented change detection approach for high-resolution remote sensing images based on multiscale fusion", Journal of Applied Remote Sensing, vol. 7, no. 1, **(2013)**.
[6] H. B. Wang, Z. Chen, X. Wang and Y. Ma, "Random finite sets based UPF-CPHD multi-object tracking", Journal of China Institute of Communications, vol. 33, no. 12, **(2012)**, pp.147-153.
[7] R. Y. Tsai and T. S. Huang, "Multiframe image restoration and registration", Advances in computer vision and Image Processing, vol. 1, no. 2, **(1984)**, pp. 317-339.
[8] J. Salvador, A. Kochale and S. Schweidler, "Patch-based spatio-temporal super-resolution for video with non-rigid motion", Signal Processing: Image Communication, vol. 28, no. 5, **(2013)**, pp. 483-493.
[9] M. S. Alam, J. G. Bognar and R. C. Hardie, "Infrared image registration and high-resolution reconstruction using multiple translationally shifted aliased video frames", IEEE Trans. Instrumentation and Measurement, vol. 49, no. 5, **(2000)**, pp. 915-923.
[10] M. Irani and S. Peleg, "Improving resolution by image registration", CVGIP: Graphical models and image processing, vol. 53, no. 3, **(1991)**, pp. 231-239.
[11] B. C. Tom and A. K. Katsaggelos, "Resolution enhancement of video sequences using motion compensation", IEEE conference on Image Processing, , lausanne, Switzerland, **(1996)** September16-19.
[12] R. C. Hardie, K. J. Barnard and E. E. Armstrong, "Joint MAP registration and high-resolution image estimation using a sequence of undersampled images", IEEE Trans. Image Processing, vol. 6, no. 12, **(1997)** , pp. 1621-1633.
[13] A. Y. Shi, C. R. Huang, M. X. Xu and F. C. Huang, "Image Super-Resolution Fusion Based on Hyperacutiy Mechanism and Half Quadratic Markov Random Field", Intelligent Automation & Soft Computing , vol. 17, no. 8, **(2011)**, pp.1167-1178.
[14] W. T. Freeman, E. C. Pasztor and O. T. Carmichael, "Learning low-level vision", International journal of computer vision, vol. 40, no. 1, **(2000)**., pp. 25-47
[15] H. He and L. P. Kondi, "An image super-resolution algorithm for different error levels per frame", IEEE Trans. Image Processing, vol. 15, no. 3, **(2006)**, pp. 592-603.
[16] M. K. Ng, H. Shen and E. Y. Lam, "A total variation regularization based super-resolution reconstruction algorithm for digital video", EURASIP Journal on Advances in Signal Processing **(2007)**.
[17] S. Farsiu, M. D. Robinson and M. Elad, "Fast and robust multiframe super resolution", IEEE Trans. Image processing, vol. 13, no. 10, **(2004)**, pp. 1327-1344.
[18] X. Li, Y. Hu and X. Gao, "A multi-frame image super-resolution method", Signal Processing, vol. 90, no. 2, **(2010)**, pp. 405-414.
[19] Q. Yuan, L. Zhang and H Shen, "Multiframe super-resolution employing a spatially weighted total variation model", IEEE Trans. Circuits and Systems for Video Technology, vol. 22, no. 3, **(2012)**, pp. 379-392.
[20] V. Patanavijit and S. Jitapunkul, "A Robust Iterative Multiframe Super-Resolution Reconstruction using a Huber Bayesian Approach with Huber-Tikhonov Regularization", the International Symposium on Intelligent Signal Processing and Communications, Yonago, Japan, **(2006)**,
[21] V. Patanavijit and S. Jitapunkul, "A Lorentzian stochastic estimation for a robust iterative multiframe super-resolution reconstruction with Lorentzian-Tikhonov regularization", EURASIP Journal on Advances in Signal Processing, **(2007)**.
[22] T. Q. Pham, L. J. Vliet and K. Schutte, "Robust super-resolution by minimizing a Gaussian-weighted L2 error norm", Journal of Physics: Conference Series. IOP Publishing, vol. 124, no. 1, 012037, **(2008).**
[23] V. Patanavijit and S. Jitapunkul, "A Tukey's biweight bayesian approach for a robust iterative SRR of image sequences", IEEE Region 10 Annual International Conference, Proceedings/TENCON, Taipei, Taiwan, **(2007)** October 30 - November 2,.
[24] S. C. Park, M. K. Park and M. G. Kang, "Super-resolution image reconstruction: a technical overview", IEEE Signal Processing Magazine, vol. 20, no. 3, **(2003)**, pp. 21-36.
[25] M. Elad and Y. Hel-Or, "A fast super-resolution reconstruction algorithm for pure translational motion and common space-invariant blur", IEEE Transactions on Image Processing, vol. 10, no. 8, **(2001)**, pp. 1187-1193.
[26] M. J. Black and A. Rangarajan, "On the unification of line processes, outlier rejection, and robust statistics with applications in early vision", International Journal of Computer Vision, vol. 19, no. 1, **(1996)**, pp. 57-91**.**

[27] N. A. El-Yamany and P. E. Papamichalis, "Using bounded-influence M-estimators in multi-frame super-resolution reconstruction: A comparative study", 15th IEEE International Conference on Image Processing, San Diego, CA, United states, **(2008)** October 12-15,
[28] P. J. Rousseeuw and A. M. Leroy, "Robust regression and outlier detection", John Wiley & Sons **(2005)**.
[29] N. X. Nguyen, "Numerical algorithms for image super-resolution", California: Stanford University **(2000)**.
[30] A. N. Tikhonov, V. I. Arsenin and F. John, "Solutions of ill-posed problems", Washington, DC: Winston, **(1977)**.

